Journal of Material Science and Mechanical Engineering (JMSME)
p-ISSN: 2393-9095; e-ISSN: 2393-9109; Volume 3, Issue 2; January-March, 2016 pp. 59-64

http://www.krishisanskriti.org/Publication.html

On the Steady-State Performance Characteristics of Finite Herringbone Grooved Journal Bearing Lubricated with Couple Stress Fluids

Arun Kumar Dinda[1] and Sisir Kumar Guha[2]

[1]*Post-graduate student, Indian Institute of Engineering Science and Technology, Howrah – 711103, W.B., India*
[2]*Mechanical Engineering, Indian Institute of Engineering Science and Technology, Howrah-711103, W.B., India*
E-mail: [1]dinda.arun@gmail.com, [2]sk_guha@rediffmail.com

Abstract—*The objective of the present paper is to theoretically investigate the steady-state performance characteristics of herringbone grooved journal bearing of finite width, lubricated with couple stress fluids. In this analysis, Stokes' micro-continum theory and the continuity equation are used. The numerical solution of the modified Reynolds equation has yielded the distribution of film pressure which determines the steady-state performance characteristics in terms of load capacity, end flow rate and frictional parameter at various values of eccentricity ratio, coupled stress parameter, helix angle and number of grooves.*

Keywords*: Hydrodynamic lubrication; steady-state; couple stress fluids; herringbone grooved journal bearing.*

1. INTRODUCTION

The problem of noise is often faced by rolling contact bearings operating at high speeds. The herringbone grooved journal bearings have less noise and high stability characteristics operating at high speeds. Performance is enhanced if couple stress fluids are used as lubricant. Vohr and Chow [1] analyzed herringbone grooved gas lubricated journal bearing with narrow groove theory (NGT), which gives fairly accurate results for large number of groove-ridge pairs at lower eccentricity ratios. Hamrock and Fleming [2] determined the optimal parameters for the herringbone-grooved journal bearing for maximum radial load capacity. Cunningham et al. [3] experimentally carried out load capacity and power loss of herringbone grooved gas lubricated journal bearings. Bootsma [4] analyzed a herringbone grooved journal bearing using the narrow groove theory. Bootsma and Tielemans [5] carried out experimental investigations on conditions of leakage free operation in herringbone grooved journal bearings. Murata et al. [6] presented a two-dimensional analysis for the flow of the lubricating film around the HGJB. Kawabata et al. [7] analyzed the regular and reversible type HGJBs based on NGT. Kinouchi and Tanaka [8] investigated static and dynamic analysis of HGJBs and compared the bearing characteristics with increasing eccentricity ratio. Kang et al. [9] presented a numerical analysis of static and dynamic characteristics and evaluated the mass parameter (a measure of stability) of oil-lubricated herringbone grooved journal bearings with 8 circular-profile grooves on the sleeve. Zirkelback and San Andres [10] performed a parametric study of a herringbone grooved journal bearing. Jang and Chang [11] analyzed the HGJBs considering cavitation effects. Faria MTC [12] analyzed performance characteristics of high speed gas lubricated herringbone groove journal bearings. Lee TS et al. [13] analyzed liquid-lubricated herringbone grooved journal bearings. Gad et al. [14] introduced the beveled-step groove profile. Liu J and Mochimaru Y [15] analyzed oil-lubricated herringbone grooved journal bearing with trapezoidal cross-section, using a spectral finite difference method. Schiffmann J and Favrat D [16] analyzed the effect of real gas on the properties of herringbone grooved journal bearings.

The conventional lubrication theory neglects the size effects of the fluid particles. The Stokes micro-continuum theory [17] is the simplest allowing the polar effects such as the presence of couple stresses [18]. A number of studies have been carried out using the Stokes microcontinum theory to investigate the effects of the couple stress parameter, 'l', on the performance of different types of fluid film bearings. Sinha P and Singh C [19] investigated couple stresses in the lubrication of rolling contact bearings considering cavitation. The performance characteristics of hydrodynamic journal bearings using lubricants with couple stress have been studied by many researchers. Sinha P, Singh C and Prasad KR [20] investigated couple stresses in journal bearing lubricants and the effects of cavitations. Lin JR [21] investigated effects of couple stresses on the lubrication of finite journal bearing. The effects of couple stresses are observed to reduce the friction parameter and result in longer bearing life. Lin JR [22] observed static characteristics of rotor bearing system lubricated with couple stress fluids. Lin JP [23] analyzed effects of couple stress on the lubrication of finite journal bearing. Mokhiamer et al. [24] investigated the effects of the couple stress parameter on the static characteristics of finite journal bearings with flexible bearing linear material. Elsharkawy et al. [25] presented an inverse solution for a finite journal bearing lubricated by a couple stress fluids. Nadivinamani NB et al. [26] analyzed hydrodynamic lubrication of rough slider bearing with couple stress fluids. Chiang HL et al. [27] studied Lubrication performance of finite journal bearings considering effects of couple stresses and surface roughness.

So far there is no investigation available that addresses the steady state performance characteristics couple stress fluid lubricated herringbone grooved journal bearing.

Nomenclature

ρ	Density of the fluid
∇	Gradient operator
h	Oil film thickness
b	Body force per unit mass
c	Body couple per unit mass
C	Clearance width in journal bearing
L	Bearing length
l	Couple-stress parameter
M	Mass of journal
P	Pressure
R	Journal radius
U, V	Tangential and normal velocity component of the journal surface
x, y, z	Coordinates
u, v, w	Fluid velocity along the x, y and z axis
η	Material constant responsible for the couple stress property
μ	Viscosity coefficient of a couple stress lubricant
c_g	Groove depth[m]
L/D	Length to diameter ratio
$\varepsilon = e/c$	Eccentricity ratio
ϕ	Attitude angle
e_x, e_y	Eccentricities in X and Y directions, respectively
γ	Groove helix angle
N_g	Number of grooves
h_{cav}	Film thickness at the point of cavitation

2. ANALYSIS

Schematic diagram of a herringbone grooved hydrodynamic journal bearing with the circumferential coordinate system used in the analysis is shown in Fig. 1. The journal operating with a steady-state eccentricity ratio ε_0 rotates with a rotational speed ω about its axis.

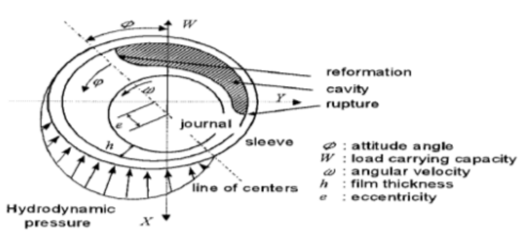

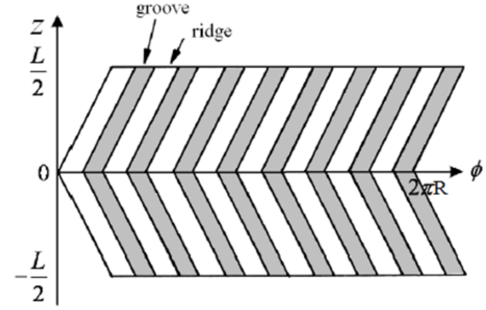

Fig. 1: Schematic diagram herringbone grooved hydrodynamic journal bearing.

Following Reynolds' equation incorporating the cavitation and mass conservation the basic governing equation in non-dimensional form, with the following substitutions

$x = R\theta$, $\bar{Z} = \dfrac{2Z}{L}$, $\bar{P} = \dfrac{pC^2}{\mu\omega R^2}$, $\bar{h} = \dfrac{h}{C}$, $\bar{l} = \dfrac{l}{C}$ is

$$\frac{\partial}{\partial\theta}\left[\bar{\phi}\left(\bar{h},\bar{l}\right)\frac{\partial\bar{p}}{\partial\theta}\right]+\left(\frac{D}{L}\right)^2\times\frac{\partial}{\partial\bar{Z}}\left[\bar{\phi}\left(\bar{h},\bar{l}\right)\frac{\partial\bar{p}}{\partial\bar{Z}}\right]=6\frac{\partial\bar{h}}{\partial\theta}\text{........(1)}$$

$$where,\bar{\phi}\left(\bar{h},\bar{l}\right)=\bar{h}^3-12\bar{h}\bar{l}^2+24\bar{l}^3\tanh\left(\frac{\bar{h}}{2\bar{l}}\right)$$

Now we use the axis transformation:

$$\theta = \xi + \frac{s}{\left(\frac{D}{L}\right)\tan\gamma} \quad \& \quad \bar{z} = s\,;$$

$$\frac{\partial}{\partial\xi}\left[\left(\bar{\phi}\frac{\partial\bar{p}}{\partial\xi}\right)+\frac{1}{\tan^2\gamma}\left(\bar{\phi}\frac{\partial\bar{p}}{\partial\xi}\right)-\frac{\left(\frac{D}{L}\right)}{\tan\gamma}\left(\bar{\phi}\frac{\partial\bar{p}}{\partial s}\right)\right]$$

$$+\left(\frac{D}{L}\right)^2\frac{\partial}{\partial s}\left[-\frac{1}{\left(\frac{D}{L}\right)\tan\gamma}\left(\bar{\phi}\frac{\partial\bar{p}}{\partial\xi}\right)+\left(\bar{\phi}\frac{\partial\bar{p}}{\partial s}\right)\right]=6\frac{\partial\bar{h}}{\partial\xi}\cdots\cdots(2)$$

Let, $A = 1+\dfrac{1}{\tan^2\gamma} = \operatorname{cosec}^2\gamma$, $B = \dfrac{\left(\frac{D}{L}\right)}{\tan\gamma} = \dfrac{\lambda}{\tan\gamma}$

$$where,\lambda=\left(\frac{D}{L}\right), C=\frac{1}{\left(\frac{D}{L}\right)\tan\gamma}=\frac{1}{\lambda\tan\gamma}$$

$$\frac{\partial\bar{\phi}}{\partial\bar{h}} = \phi',(say) \text{ and } \chi = \frac{\phi'}{\phi}$$

Non-dimensional film thickness $\bar{h} = 1+\bar{c}_g+\varepsilon_x\cos\left(\xi_i-\varphi_0\right)+\varepsilon_y\sin\left(\xi_i-\varphi_0\right)$

Where, $\varepsilon_x = \varepsilon_0 \cos\varphi$ and $\varepsilon_y = \varepsilon_0 \sin\varphi$

$$or,\ A\left(\frac{\partial^2 \bar{p}}{\partial \xi^2}\right)+\lambda^2\left(\frac{\partial^2 \bar{p}}{\partial z^2}\right)+A\chi\left(-\varepsilon_x \sin(\xi-\varphi_0)+\varepsilon_y \cos(\xi-\varphi_0)\right)\frac{\partial \bar{p}}{\partial \xi}$$

$$-B\chi\left(-\varepsilon_x \sin(\xi-\varphi_0)+\varepsilon_y \cos(\xi-\varphi_0)\right)\frac{\partial \bar{p}}{\partial z}-\left(B+C\lambda^2\right)\left(\frac{\partial^2 \bar{p}}{\partial z \partial \xi}\right)$$

$$=\frac{6}{\phi}\left(-\varepsilon_x \sin(\xi-\varphi_0)+\varepsilon_y \cos(\xi-\varphi_0)\right) \text{.............}(3)$$

2.1. Numerical solution for pressure

Equation (3) is discretized by the finite difference method and solved by Gauss-Seidel iterative method with successive over-relaxation scheme to obtain the steady state pressure distribution $\bar{p}$ satisfying the boundary conditions as given: $\bar{p}(\theta, \pm 1) = 0$ (ambient pressure at both bearing end);

$\frac{\partial \bar{p}}{\partial \bar{z}}(\theta, 0) = 0$ (symmetrical pressure at the mid- plane);

$\frac{\partial \bar{p}}{\partial \theta}(\theta_c, \bar{z}) = 0$; $\bar{p}(\theta, \bar{z}) = 0$ for $\theta \geq \theta_c$

(cavitation condition).

The bearing surface area is divided into a number of rectangular meshes of size $(\Delta\theta \times \Delta\bar{z})$ each. Representing a grid point (i,j), where i and j represent the co-ordinates along x(θ) and z($\bar{z}$) directions respectively.To implement the above numerical procedure, a uniform grid size is adopted in the circumferential and axial directions. For calculating film pressure at each set of input parameters, the following convergence criterion is adopted.

$$\left|1-\frac{\sum \bar{p}_{old}}{\sum \bar{p}_{new}}\right| \leq 0.0001$$

3. STEADY-STATE BEARING PERFORMANCE CHARACTERISTICS

3.1. Load Carrying Capacity

The non-dimensional radial and transverse load components are obtained by

$$\bar{W}_r = \frac{W_r C^2}{\mu\omega R^3 L} = -\int_0^{2\pi}\int_0^{L/2} \bar{p}\cos\theta\, d\theta\, d\bar{z} \quad \text{and} \quad \bar{W}_\phi = \frac{W_\phi C^2}{\mu\omega R^3 L} = \int_0^{2\pi}\int_0^{L/2} \bar{p}\sin\theta\, d\theta\, d\bar{z}$$

Non-dimensional steady state load is computed as:

$$\bar{W}_0 = \left[\left(\bar{W}_r\right)^2 + \left(\bar{W}_\phi\right)^2\right]^{\frac{1}{2}} \cdots\cdots\cdots\cdots\cdots\cdots (4)$$

3.2. End Flow Rate

The volume flow rate in non-dimensional form is given by:

$$\bar{Q} = \frac{QL}{\omega R^3 C} = \frac{1}{3}\int_0^{2\pi} \frac{\partial \bar{p}}{\partial \bar{z}}\left(\bar{\phi}\left(\bar{h}, \bar{l}\right)\right) d\xi \cdots\cdots\cdots\cdots (5)$$

3.4. Frictional Parameter

The non-dimensional frictional force is given by

$$\bar{F} = \bar{F}_s + \bar{F}_{sc}$$

$$= \int_0^{\theta}\left[\frac{1}{\bar{h}} + \frac{\bar{h}}{2}\frac{\partial \bar{p}}{\partial \xi}\right] d\xi + \int_{\theta}^{2\pi}\left(\frac{\bar{h}_{cav}}{\bar{h}}\right)\left[\frac{1}{\bar{h}} + \frac{\bar{h}}{2}\frac{\partial \bar{p}}{\partial \xi}\right] d\xi \cdots\cdots\cdots (6)$$

The frictional parameter is consequently obtained as follows: $f\left(\frac{R}{C}\right) = \frac{\bar{F}}{\bar{W}}$

4. RESULTS AND DISCUSSION

From the equation denoted by (3) it is obvious that the film pressure distribution depends on the parameters, namely, *L/D*, ε_0, $\bar{l}$, *Ng* and γ. A parametric study has been carried out for all the above mentioned parameters excepting *L/D* which has been fixed at 1.0.

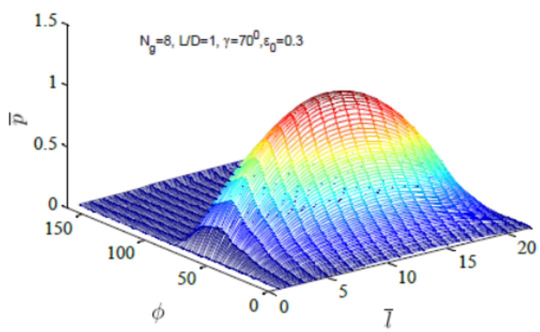

Fig. 2. Pressure Distribution

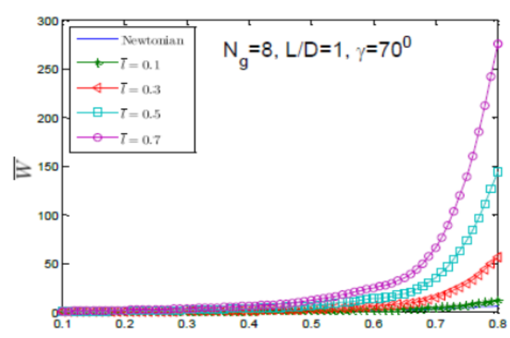

Fig.3.variation of $\bar{W}$ with ϵ_0 for various values of $\bar{l}$

4.1. Load Carrying Capacity, W

4.1.1. Effect of eccentricity ratio at different values of couple stress characteristics length

Fig.3. Shows the variation of load capacity with eccentricity ratio for various values of couple stress characteristics length (

$\bar{l}$). It's found on increase of eccentricity ratio (ε_0), increases the load capacity at any value of ($\bar{l}$). Moreover, the figure reveals load capacity increases with increase of ($\bar{l}$) and approaches asymptotically to the Newtonian value as $\bar{l}\rightarrow 0$. The physical reason for the above observation is as $\bar{l}$ tends to higher value, the viscous shear stress in the fluid around the suspended particles of additives increases by the spinning or coupling effect.

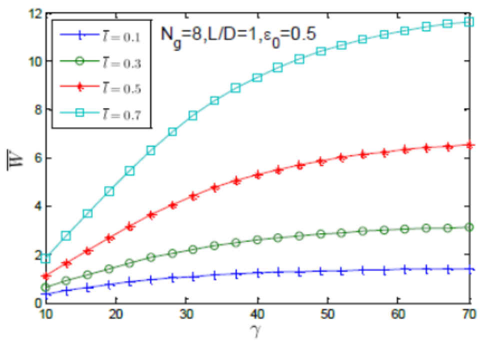

Fig.4.variation of $\overline{W}$ with γ for various values of $\bar{l}$

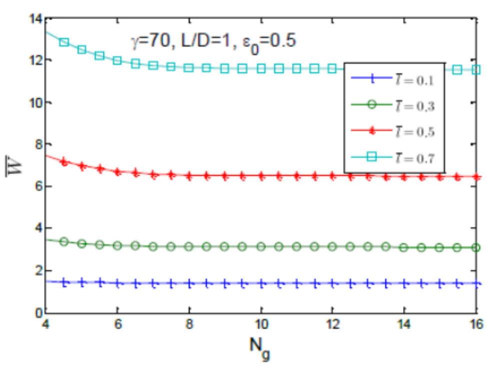

Fig.5.variation of $\overline{W}$ with N_g for various values of $\bar{l}$

4.1.2. Effect of helix angle at different values of couple stress characteristics length

Fig.4. Shows the variation of load capacity with helix angle for various values of couple stress characteristics length ($\bar{l}$). It's found on increase of helix angle (γ), increases the load capacity at any value of ($\bar{l}$). Moreover, the figure reveals load capacity increases with increase of ($\bar{l}$). The physical reason for the above observation is as ($\bar{l}$) tends to higher value, the viscous shear stress in the fluid around the suspended particles of additives increases by the spinning or coupling effect.

4.1.3. Effect of groove number at different values of couple stress characteristics length

Fig.5. Shows the variation of load capacity with groove number for various values of couple stress characteristics length ($\bar{l}$). It's found on increase of groove number (N_g) the load capacity does not vary significantly at any value of ($\bar{l}$).

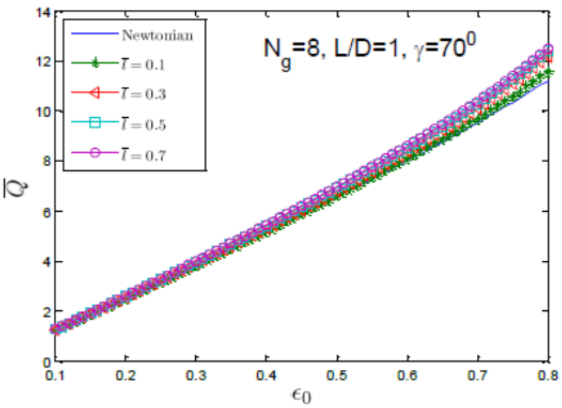

Fig.6.variation of $\overline{Q}$ with ϵ_0 for various values of $\bar{l}$

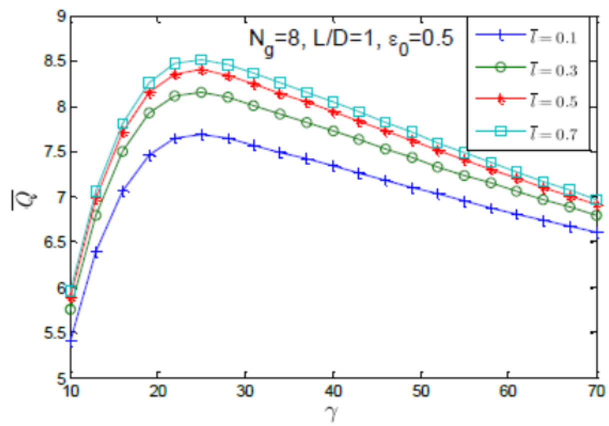

Fig.7.variation of $\overline{Q}$ with γ for various values of $\bar{l}$

4.2. End flow rate, Q

4.2.1. Effect of eccentricity ratio at different values of couple stress characteristics length

Fig.6. Shows the variation of end flow rate with eccentricity ratio for various values of couple stress characteristics length ($\bar{l}$). It's found on increase of eccentricity ratio (ε_0), increases the end flow rate at any value of $\bar{l}$.

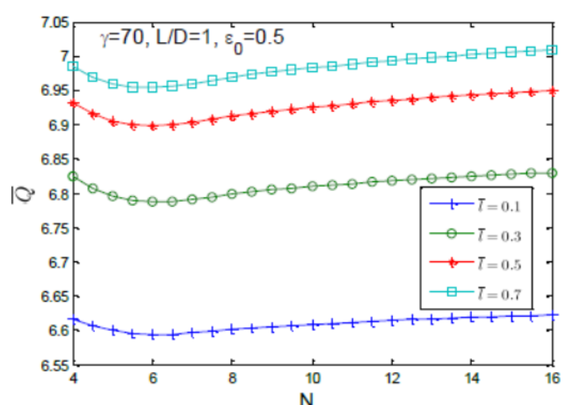

Fig.8.variation of $\overline{Q}$ with N_g for various values of $\bar{l}$

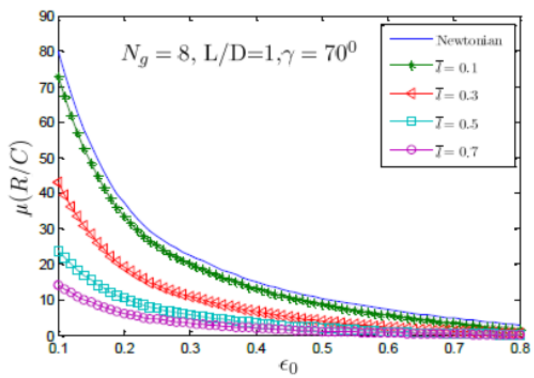

Fig.9.variation of $\mu(R/C)$ with ϵ_0 for various values of $\bar{l}$

Moreover, the figure reveals end flow rate increases by small amount with increase of $\bar{l}$ and approaches asymptotically to the Newtonian value as $\bar{l}\rightarrow 0$. The physical reason for the above observation is as $\bar{l}$ tends to higher value, the viscous shear stress in the fluid around the suspended particles of additives merely effects on end flow rate.

4. 2.2.Effect of helix angler at different values of couple stress characteristics length

Fig.7. Shows the variation of end flow rate with helix angle*(γ)* for various values of couple stress characteristics length ($\bar{l}$).It's found on increase of helix angle *(γ)*, the end flow rate initially increases , then attains a maximum value, then decreases at any value of*($\bar{l}$)*.

4. 2.3.Effect of groove number at different values of couple stress characteristics length

Fig.8. Shows the variation of end flow rate with groove number for various values of couple stress characteristics length *($\bar{l}$)*. It's found on increase of groove number *(N_g)*, the end flow rate initially slowly decreases, and then slowly increases at any value of *($\bar{l}$)*.

4.3. Frictional parameter

4.3.1. Effect of eccentricity ratio at different values of couple stress characteristics length

Fig.9. Shows the variation of frictional parameter with eccentricity ratio for various values of couple stress characteristics length *($\bar{l}$)*. It's found on increase of eccentricity ratio *(ε_0)*, decrease the frictional parameter at any value of *($\bar{l}$)*. Moreover, the figure reveals frictional parameter decreases with increase of *($\bar{l}$)* and approaches asymptotically to the Newtonian value as $\bar{l}\rightarrow 0$.

4.3.2. Effect of helix angle at different values of couple stress characteristics length

Fig.10. shows the variation of frictional parameter with helix angle *(γ)*. It's found on increase of helix angle *(γ)*, the frictional parameter decreases at any value of *($\bar{l}$)*.

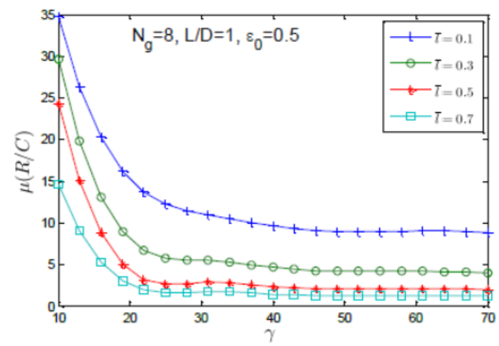

Fig.10.variation of $\mu(R/C)$ with γ for various values of $\bar{l}$

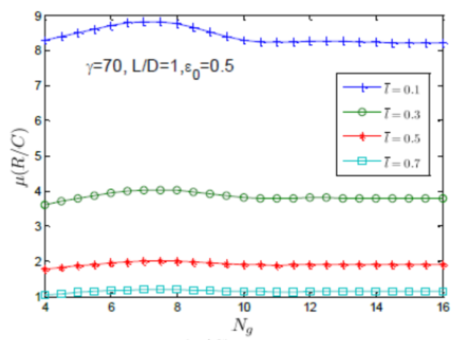

Fig.11.variation of $\mu(R/C)$ with N_g for various values of $\bar{l}$

4.3.3. Effect of groove number at different values of couple stress characteristics length

Fig.11. Shows the variation of frictional parameter with eccentricity ratio for various values of couple stress characteristics length ($\bar{l}$).It's found on increase of groove number *(N_g)*, the frictional parameter does not vary significantly at any value of *($\bar{l}$)*.

5. CONCLUSIONS

From the results of this study, the following conclusions can be drawn:

According to the results obtained for a particular value *L/D*=1.0, the influences of various parameters on the static performance characteristics can be highlighted as follows.

Load capacity increases with increase of eccentricity ratio at different values of couple stress characteristics length. Moreover, couple stress fluids exhibit a better load capacity than a Newtonian fluid under steady-state condition.

The effect of helix angle is to improve the load capacity at different values of couple stress characteristics length.

Load capacity is not affected significantly with increase of number of grooves at different values of couple stress characteristics length.

End flow rate increases with increase of eccentricity ratio at different values of couple stress characteristics length. Moreover, couple stress fluids exhibit an end flow rate nearly similar to Newtonian fluid under steady-state condition.

The effect of helix angle is to increase the end flow rate at different values of couple stress characteristics length up to around 25^0.Then it improves significantly.

End flow rate is not affected significantly with increase of number of grooves at different values of couple stress characteristics length. But as couple stress characteristics length increases end flow rate also increases.

Frictional parameter decreases with increase of eccentricity ratio at different values of couple stress characteristics length, approaching asymptotically to the Newtonian value. Moreover, Moreover, couple stress fluids exhibit a better frictional parameter than a Newtonian fluid under steady-state condition.

The effect of helix angle is to decrease the frictional parameter at different values of couple stress characteristics length.

Frictional parameter is not affected significantly with increase of number of grooves at different values of couple stress characteristics length. But as couple stress characteristics length $(\bar{l})$ increases frictional parameter also increases.

REFERENCES

[1] Vohr JH, Chow CY. Characteristics of Herringbone grooved gas lubricated journal bearings. ASME J. Basic Engg. 87; 1965. p. 568–578.

[2] Hamrock BJ, Fleming DP. Optimization of self-acting herringbone grooved journal bearings for maximum radial load capacity. Proceedings of the fifth gas bearing symposium. University of Southampton; 1971. p. 13.1-13.17.

[3] Cunningham RE, Fleming DP, Anderson WJ. Experimental load capacity and power loss of herringbone grooved gas lubricated journal bearings. J. Lub. Technol. 93; 1971. p. 415–422.

[4] Bootsma J. Liquid-lubricated spiral-groove bearings. phillips research reports-supplements. No. 7. The Netherlands; 1975.

[5] Bootsma J, Tielemans LP. Conditions of leakage free operation in herringbone grooved journal bearings. ASME J. Lubr. Technol. 99; 1977.p. 213–223.

[6] Murata S, Miyake Y, Kawabata N. Two-dimensional analysis of herringbone groove journal bearings. JSME. 23; 1980. p. 1120–1227.

[7] Kawabata N, Ozawa Y, Kamaya S, Miyake Y. Static characteristics of the regular and reversible rotation type herringbone grooved journal bearing. ASME J. Tribol.111; 1989. p. 484–490.

[8] Kinouchi K, Tanaka K. Performance characteristics of herringbone grooved journal bearings using a finite element method. Proceedings of the japan international tribology conference, II; 1990. p. 935–940.

[9] Kang K, Rhim Y, Sung K. A study of the oil-lubricated herringbone-grooved journal bearing-part 1: Numerical analysis. ASME J.Tribol. 118; 1996. p. 906–911.

[10] Zirkelback N, San Andres L. Finite element analysis of herringbone groove journal bearings: a parametric study. ASME journal of tribology. Vol.120; 1998. p. 234–240.

[11] Jang GH, Chang DI. Analysis of hydrodynamic herringbone grooved journal bearing considering cavitation. ASME J. Tribol. 122; 2000 .p. 103–109.

[12] Faria MTC. Some performance characteristics of high speed gas lubricated herringbone groove journal bearings. JSME Int. J. Ser. C 44; 2001. p. 775–781.

[13] Lee TS, Liu YG, Winoto SH. Analysis of liquid-lubricated herringbone grooved journal bearings. International journal for numerical methods for heat & fluid flow. 14(3); 2004.p. 341-65.

[14] Gad AM, Nemat-Alla M, Khalil AA, Nasr A. On the oiptimum groove geometry for herringbone grooved journal bearings. ASME J. Tribol.128; 2006. p. 585–593.

[15] Liu J, Mochimaru Y. Analysis of oil-lubricated herringbone grooved journal bearing with trapezoidal cross-section, using a spectral finite difference method. Journal of hydrodynamics. vol. 22, no. 5, supplement 1; 2010. p. 408–412.

[16] Schiffmann J, Favrat D. The effect of real gas on the properties of herringbone grooved journal bearings. Tribol. Int. 43; 2010. p. 1602–1614.

[17] Ariman TT, Sylvester ND. Application of micro-continum fluid mechanics. Int. J. Eng. Sci. 12; 1974.p. 273-293.

[18] Stokes VK. Couple stresses in fluids. Phys. Fluid. 9; 1966.p. 1709-1715.

[19] Sinha P, Singh C. Couple stresses in the lubrication of rolling contact bearings considering cavitation. Wear. 67; 1981.p. 85-98.

[20] Sinha P, Singh C, Prasad KR. Couple stresses in journal bearing lubricants and the effects of cavitations. Wear. 67; 1981.p.15-24.

[21] Lin JR. Effects of couple stresses on the lubrication of finite journal bearing. Wear. Vol. 206; 1997. p. 171-178.

[22] Lin JR. Static characteristics of rotor bearing system lubricated with couple stress fluids. Comput. Struct. Vol. 62. No. 1; 1997 p. 175-184.

[23] Lin JP. Effects of couple stress on the lubrication of finite journal bearing. Wear. Vol. 206; 1997. p. 171 –178.

[24] Mokhiamer UM, Crosby WA, El-Gamal HA. A study of a journal bearing lubricated by fluids with couple stress considering the elasticity of the liner. Wear. Vol. 224; 1999. p. 191-201.

[25] Elshakawy A, Guedouar LH. An inverse solution for finite bearings lubricated with couple stress fluids. J. Tribology Int. 34; 2001.p.107-118.

[26] Nadivinamani NB, Fathima S, Hiremath PS**.** Hydrodynamic lubrication of rough slider bearing with couple stress fluids. Tribology International,Vol. 36; 2003.p.949-959.

[27] Chiang HL, Lin JR, Hsu CH. Lubrication performance of finite journal bearings considering effects of couple stresses and surface roughness. Tribology International. vol. 37; 2004. p. 297–307.